REPORT DOCUMENTATION PAGE

Form Approved
OMB NO. 0704-0188

1. AGENCY USE ONLY (Leave Blank)	2. REPORT DATE 02/04/2005	3. REPORT TYPE AND DATES COVERED Final Report: 01-Aug-01 - 31-Jul-04

4. TITLE AND SUBTITLE
The fabrication of Self-assembled Quantum Dot Lasers of InGaAs on Si

5. FUNDING NUMBERS
DAAD19-01-1-0690

6. AUTHOR(S)
Ya-Hong Xie, Bin Shi, ZuoMing Zhao, Jian Liu, HyungJun Kim, Oksana Hul'ko, Kyuchul Chong

7. PERFORMING ORGANIZATION NAME(S) AND ADDRESS(ES)
Dept. Mat. Sci. Eng., University of California Los Angeles
6532 Boelter Hall, Box 951595
Los Angeles, CA 90095-1595

8. PERFORMING ORGANIZATION REPORT NUMBER 2004

9. SPONSORING / MONITORING AGENCY NAME(S) AND ADDRESS(ES)
U. S. Army Research Office
P.O. Box 12211
Research Triangle Park, NC 27709-2211

10. SPONSORING / MONITORING AGENCY REPORT NUMBER
42457.1-EL

11. SUPPLEMENTARY NOTES
The views, opinions and/or findings contained in this report are those of the author(s) and should not be construed as an official Department of the Army position, policy or decision, unless so designated by other documentation.

12 a. DISTRIBUTION / AVAILABILITY STATEMENT
Approved for public release; distribution unlimited.

12 b. DISTRIBUTION CODE

13. ABSTRACT (Maximum 200 words) We have made significant progress both in design and fabrication of Si-based laser device structures. We have demonstrated several key parts of the laser structure including a SiGe waveguide with good optical and electrical properties for both light and carriers confinement. SiGe resonant cavity with DBRs to serve as Si-based laser cavity was design and fabricated, which is, to the best of our knowledge, the first SiGe based resonant cavity with DBRs reported thus far. In addition, we have carried out theoretical calculation for coupled SAQD systems and formulated the distinct advantage of a coupled SAQD system for laser applications. In conjunction with ARO program DAAD19-01-1-0532, we have achieved good control and the mapping of of the parameter space for fabricating InAs quantum dots on Si substrate. We have also carried out detailed transmission electron microscopy (TEM) study of individual dots and experimentally identified the critical dot size for dislocation under different growth conditions. The very small critical size of InAs SAQD for dislocation and the associated extreme quantum confinement show that there might not be a window in the dot size for which electron-hole pairs can be confined and the dots are coherently strained.

14. SUBJECT TERMS
Laser, SAQD, MBE, waveguide, resonant cavity, distributed Bragg reflectors, TEM, electron beam lithography

15. NUMBER OF PAGES
28

16. PRICE CODE

17. SECURITY CLASSIFICATION OR REPORT	18. SECURITY CLASSIFICATION ON THIS PAGE	19. SECURITY CLASSIFICATION OF ABSTRACT	20. LIMITATION OF ABSTRACT
UNCLASSIFIED	**UNCLASSIFIED**	**UNCLASSIFIED**	**UL**

Proposal title: The Fabrication of Self-assembled Quantum Dot Lasers of InGaAs on Si

ARO Contract #: DAAD19-01-1-0690

Beginning date: 11 July, 2001

ARO technical representative: Dr. Micheal D. Gerhold

Abstract

We have made significant progress both in design and fabrication of Si-based laser device structures. We have demonstrated several key parts of the laser structure including a SiGe waveguide with good optical and electrical properties for both light and carriers confinement. SiGe resonant cavity with DBRs to serve as Si-based laser cavity was design and fabricated, which is, to the best of our knowledge, the first SiGe based resonant cavity with DBRs reported thus far. In addition, we have carried out theoretical calculation for coupled SAQD systems and formulated the distinct advantage of a coupled SAQD system for laser applications. In conjunction with ARO program DAAD19-01-1-0532, we have achieved good control and the mapping of of the parameter space for fabricating InAs quantum dots on Si substrate. From both experiments and theoretical calculation, we have proved the Volmer-Weber growth mode for InAs on Si. We have also carried out detailed transmission electron microscopy (TEM) study of individual dots and experimentally identified the critical dot size for dislocation under different growth conditions. We are able to control the density and dot size uniformity of InAs SAQDs: density from 10^9 cm^{-2} to 10^{11} cm^{-2}, dot diameter from 9 nm to 30 nm, dot height from 4nm to 15nm and size distribution within 30%. The very small critical size of InAs SAQD for dislocation and the associated extreme quantum confinement show that there might not be a window in the dot size for which electron-hole pairs can be confined and the dots are coherently strained.

Highlight of Research Accomplishment

1. Laser cavity fabrication and measurement:

1). SiGe waveguide design and fabrication

To achieve the light confinement in laser device, a waveguide structure is needed in the Si-based quantum-dot (QD) laser. SiGe waveguide is a good choice due to its low loss, good coupling with fiber and flexibility of doping. For good performance, the parameters of the waveguide structure need to be optimized.

Effective refraction index method and mode counting technique were used to get the phase diagram of guided modes. In these diagrams, a safe region can be found in which only single TE mode and TM mode are supported by the structure. So we can choose any parameters in this region to meet the other requirements, such as critical thickness for strained layer without dislocations, cross section matching with single mode fiber. Also, field distribution in the waveguide was calculated by using preconditioned block-iterative eigensolvers in a planewave basis. With the field distribution (Fig.1), optimized position for active layer of QDs in the waveguide can be decided at the highest filed intensity area.

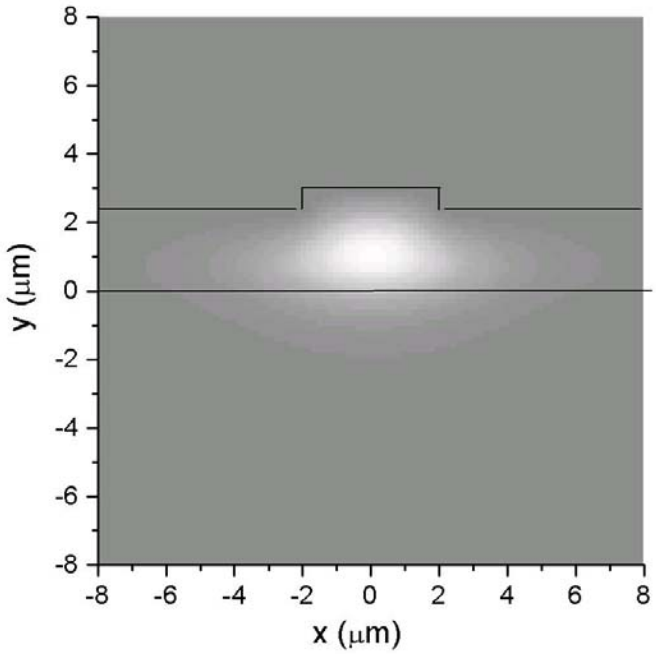

Fig.1 Cross section filed distribution in the rib waveguide.

SiGe waveguide structure with optimized parameters has been fabricated by Molecular Beam Epitaxy (MBE). Fig. 2 shows the propagation loss of the waveguide is 0.88 dB/cm, which should be compared with typical waveguide loss in semiconductor laser structures of few dB/cm. It should be pointed out that the structure we measured does have a heavily doped capping layer necessary for efficient current injection. Fig. 3 is the I-V characteristics of the waveguide structure.

Injection current more than 2 kA/cm2 can be easily achieved. So a waveguide structure with both good optical and electrical properties is achieved.

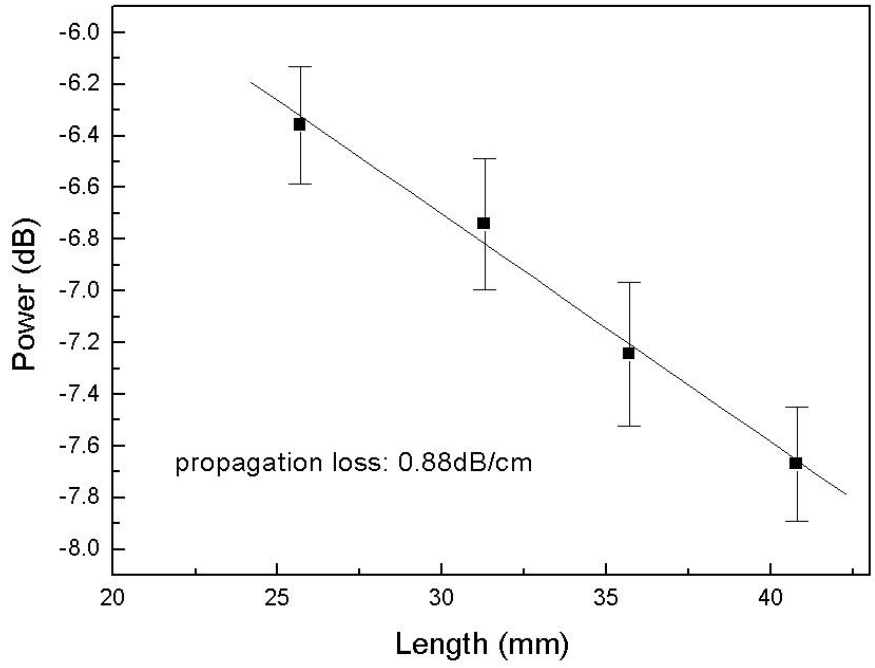

FIG. 2 Propagation power in SiGe waveguide as a function of length.

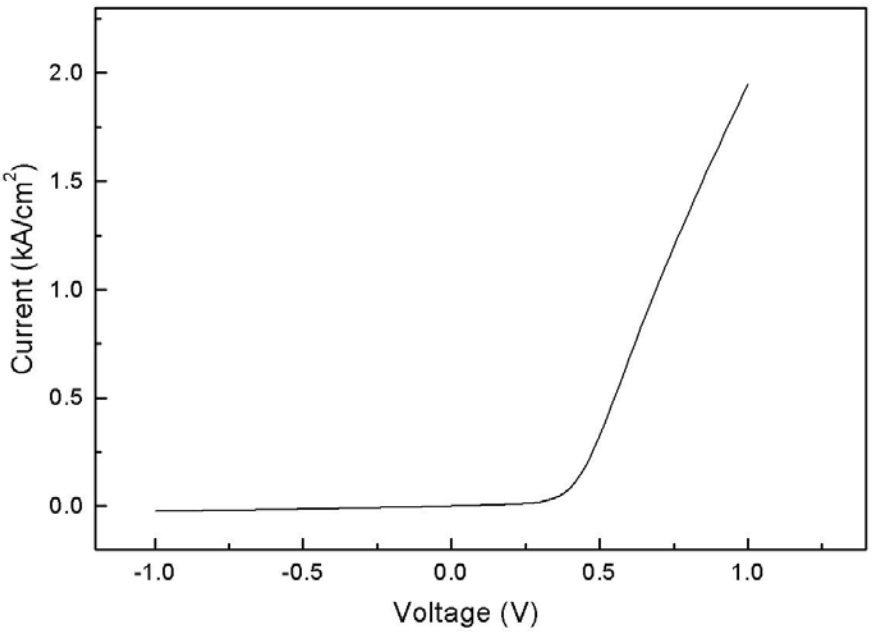

FIG. 3 Current changes with applied bias in the waveguide structure.

To understand the influence of metal layer, which will be exist as electrode in the laser device, we carried out a study of waveguide with a metal layer on the top. A 1μm thick silicon spacer (also used in the DBR cavity) is used to introduce better confinement of light inside the SiGe layer, which will decrease the free carrier absorption in the metal layer. Also such a layer will make the fully strained SiGe layer more stable. The propagation loss measure (Fig. 4) showed such a structure has a loss of 5.0dB/cm, which is very low for a metal cladding waveguide and will not cause any trouble in the laser cavity applications.

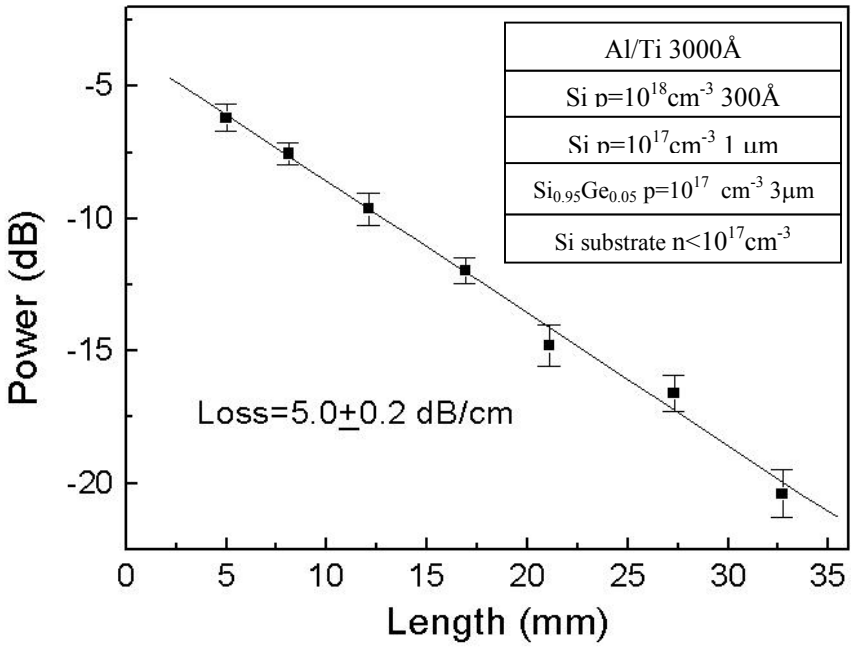

Fig.4 Propagation loss measurements of SiGe waveguide with 300nm Al layer. The waveguide structure are shown as inserts.

2). Distributed Bragg reflector (DBR) laser cavity

A high quality laser cavity for the lateral mode control is very important for the single mode operation of laser devices. Transfer matrix method with an additional gain term was used to simulate the stimulated light emission in small signal condition. Fig. 5(a) shows the emission spectrum from standard laser cavity with one layer of InAs QDs. We can find, due to the inhomogeneously broadened gain spectrum caused by size fluctuation of the quantum dots, there is a large number of longitudinal modes even in a very short cavity.

To suppress unwished longitudinal modes, the distributed Bragg reflector (DBR) laser structure was used. Phase shift condition of the cavity was also

considered in the design to obtain more suppression. Fig. 5(b) shows the stimulated emission spectrum from such a structure. Number of longitudinal modes is greatly reduced, so single mode operation can be easily achieved.

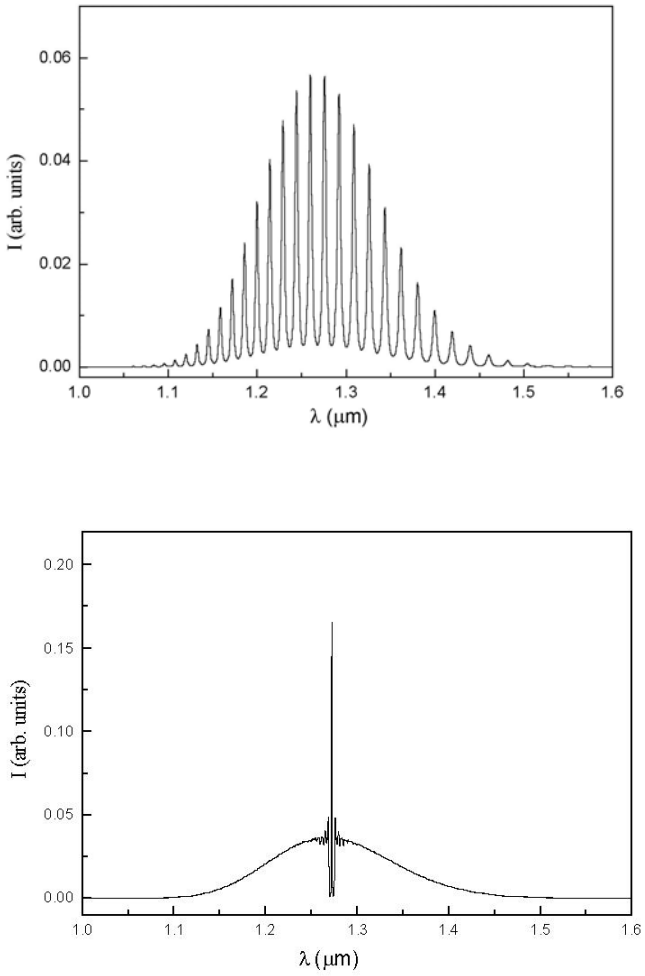

Fig.5 Stimulated emission from (a) standard cavity of l=14.4mm (b) DBR structure.

Combining the grating pattern and our optimized SiGe rib waveguide, we fabricated the SiGe resonant cavity for the laser application. Figure 6 is a SEM picture of the resonant cavity. The height of the rib is 0.7 μm, the etching thickness of the grating pattern on the waveguide is 0.3 μm, the length of the cavity is 21.84 μm, and the DBRs at both side of the cavity include 1000 periods grating, where each period is 0.56 μm.

To characterize the resonant cavity, we measure the transmission spectrum of the resonant cavity, which is shown in Fig. 7. Only one resonant mode centered at 1315.5 nm can be found in the transmission spectrum, which shows such a cavity is very suitable for single mode oscillation of SAQD lasers. From the transmission

spectrum, we can also calculate the cavity quality factor $Q = 317$ and photon lifetime $\tau_c = 0.22\,\text{ps}$, which can be further improved by increasing the number of periods in the DBRs and the etching depth of the trenches in the DBR pattern.

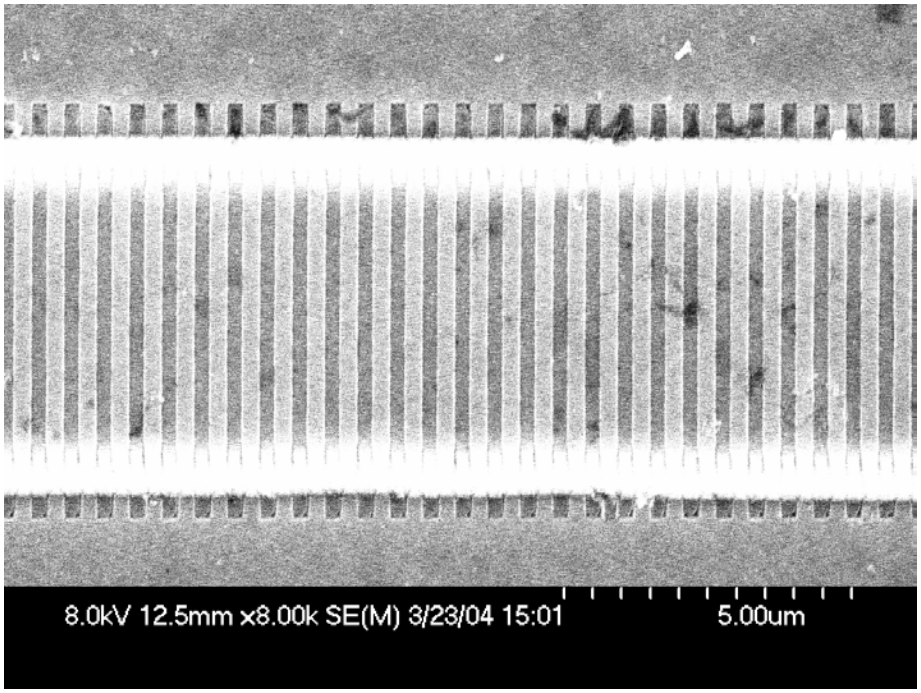

Fig. 6 Top view SEM photograph of the SiGe waveguide with DBRs.

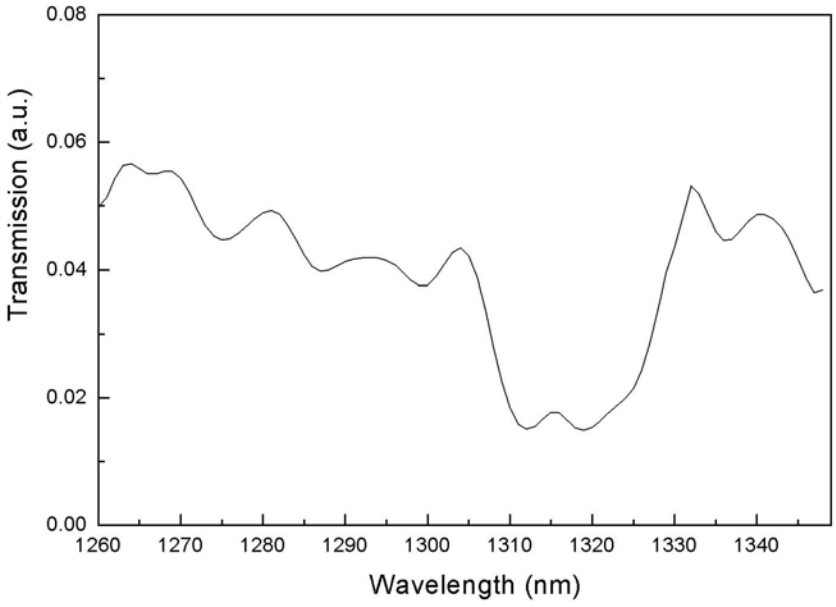

Fig. 7 Transmission spectrum of the SiGe resonant cavity with DBRs.

3). Coupling effect on the laser performance

One of the major challenges in the field of quantum dot laser is the size ununiformity of quantum dots, which will cause a broad gain peak and therefore decrease the efficiency of laser and introduce multi-mode laser operation. A lot of effort has been put into the growth of highly uniform quantum dots, but till now it is still very difficult to get a very uniform quantum dots. In this report we will show with coupling of the quantum dots, the broadening of laser spectrum can be reduced and the mode power of laser can be increased. And a system with poorer size uniformity will benefit more from the coupling, which makes coupling even more helpful for reducing the growth difficulty.

Fig. 8 shows the calculated spectra of quantum dot laser with coupled and uncoupled quantum dots. The calculation is done by solving coupled rate equation of such a quantum dot laser structure. In the results, the spectral width of the laser output of a laser structure with coupled quantum dots is significant narrower than that of a system with uncoupled quantum dots. This phenomenon can be understood by considering the group of dots that resonant with the most intense mode. Because of the higher stimulated recombination rate, they serve as a fast sink for excess carriers. Coupling allows the excess carriers from the dots with slower recombination rate to migrate into the sinks leading to a significantly enhanced emission into the strongly resonant mode and in the meantime reducing the emission into the other modes. The saturation output power of the strongest mode of the laser structure with different inhomogeneous and homogeneous broadening and different number of quantum dots layers are also calculated using coupled rate equations. The results are shown in Fig. 9, which clearly shows that the enhancement of mode power by coupling effect increases with coupled layers. Another important thing is the enhancement due to the coupling is larger in the system with poorer dot size uniformity, so the restriction of dot size uniformity can be loosed, which will reduce the growth difficulty.

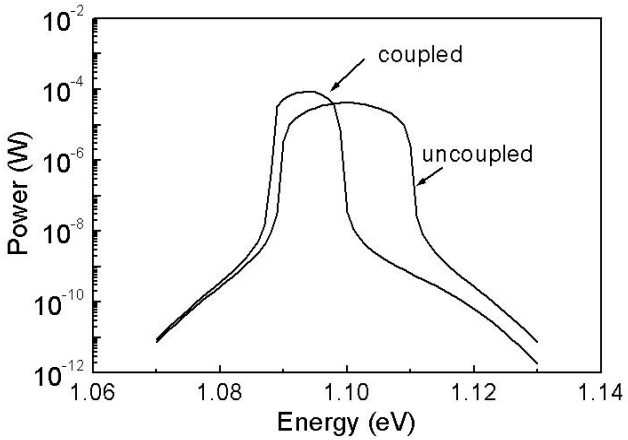

FIG.8 Calculated light emission spectra of quantum dot laser with coupled and uncoupled quantum dots.

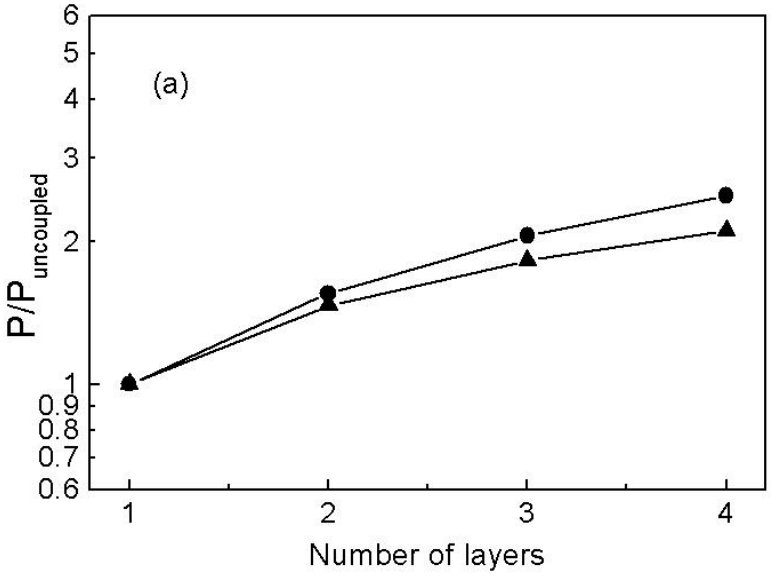

FIG. 9 Calculated enhancement of single mode output power of quantum dot laser with FWHM of inhomogeneous broadening 20meV (circles) and 10meV(up triangles).

2. III-V quantum dots on Si (001):

1). Fabrication of InAs SAQDs on Si (001): Comparing to Ge SAQDs on Si, the considerations involved in the growth of InAs SAQD on Si is quite a bit more complex. Because there is only one group in the world headed by Prof. Bimberg and Prof. Gosele of Germany that is doing serious research in the fabrication of InAs SAQD on Si, there isn't much information available in the literature. For example, the most important question of whether the growth is in Stranski-Krastanov mode (a wetting layer followed by 3D growth) or Vomer-Weber mode (non-wetting 3D growth) is not known for sure. Furthermore, the effect of As over-pressure on the dot nucleation and shape is not established, although we have been growing in the As rich regime. Finally, the critical dot size for dislocation has not been determined.

For InAs coverage dependence study

Plan-view TEM images of InAs dots with different InAs nominal coverage are shown in Figure 10. The density and size dependence on InAs coverage are shown in Figure 11. TEM results indicate that dot formation begins at very early stage of the growth (< 0.3 ML). At 0.3 ML of InAs coverage, the dot density is approximately 1.7×10^{10} cm^{-2} indicating Volmer-Weber (VW) growth mode.

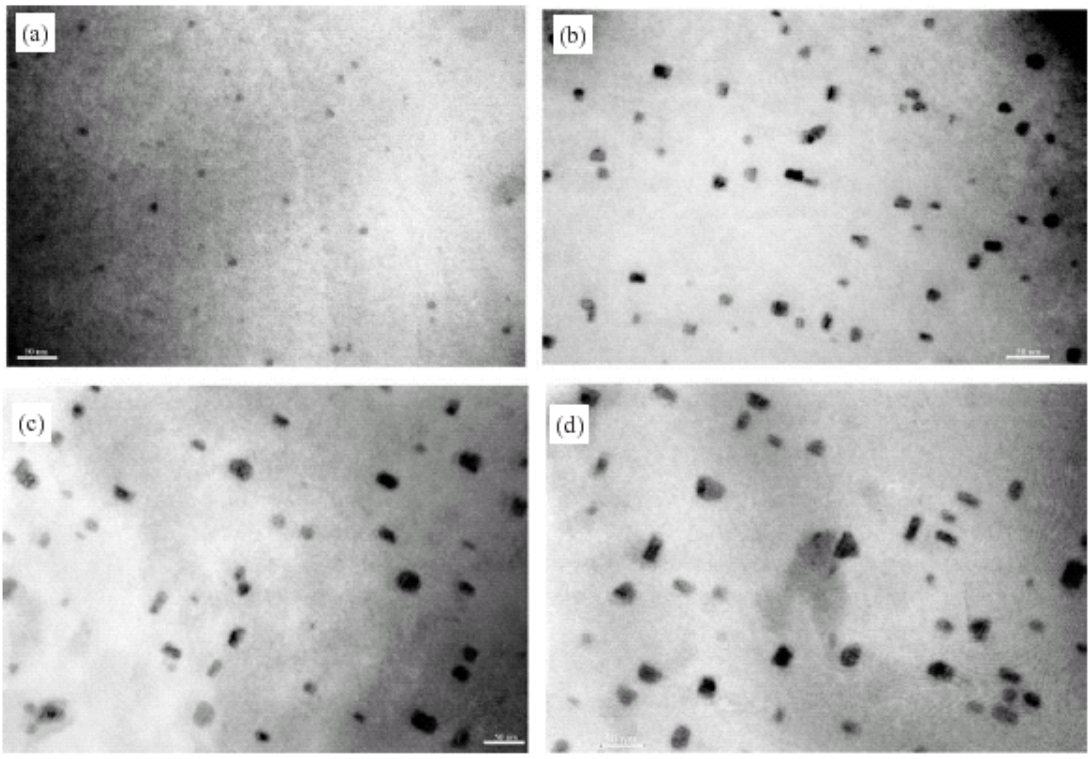

Figure 10. Bright-field plan-view TEM of InAs dots with various InAs nominal coverage (a) 0.3 ML, (b) 0.7 ML, (c) 1.0 ML, (d) 1.4 ML.

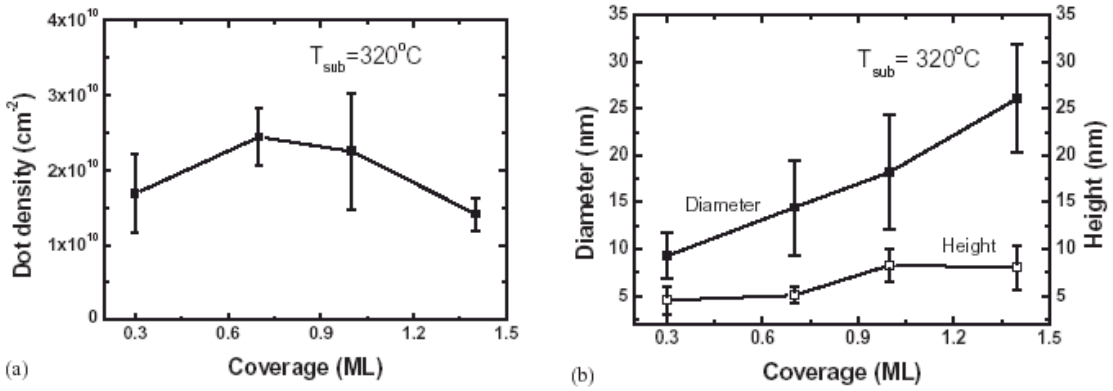

Figure 11. (a) Plot of InAs dot density dependence on the nominal coverage and (b) Plot of InAs dot size dependence on the nominal coverage.

Figure 12 shows the cross-section TEM of typical InAs dots with the different coverage. With increasing InAs coverage, not only dot size but also shape of the dots change. Most dots have an irregular shape at 0.3 ML coverage that changes to highly regular huts with (111) facets at 0.7 ML. At 1.0 ML, portion of dots evolves into dome shape with no clear facets. At 1.4 ML, nearly 100% of the dots are dome shape.

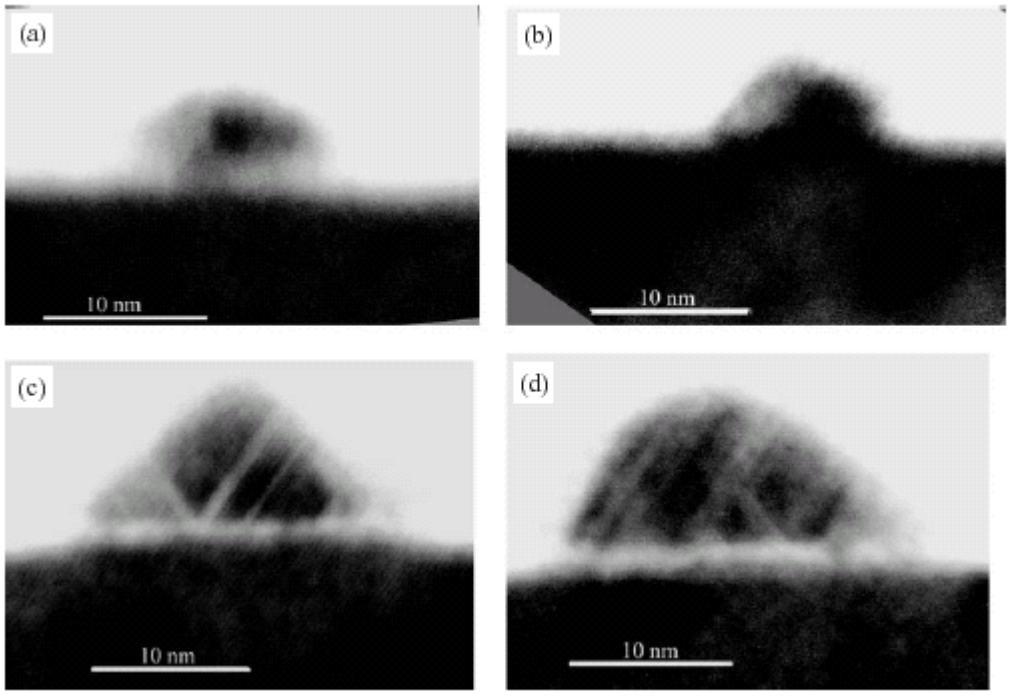

Figure 12. Bright-field cross-section TEM of typical InAs dots with different InAs nominal coverage: (a) 0.3 ML, (b) 0.7 ML, (c) 1.0 ML, (d) 1.4 ML.

For arsenic pressure dependence study

The strong dependence of dot density on As BEP is in clear contrast to its weak dependence on InAs coverage, as shown in Figure 13(a). InAs dot density increases in a near exponential fashion from 4.3×10^{9} to 1.8×10^{11} cm^{-2} as As BEP is decreased from 9.2×10^{-6} to 1.2×10^{-7} torr. InAs dot size and volume change with decreasing As BEP, as shown in Fig. 13(b). The total dot volume decreases at the low As BEP. This indicates that there are 2-dimensional InAs structures formed between dots at low As BEP.

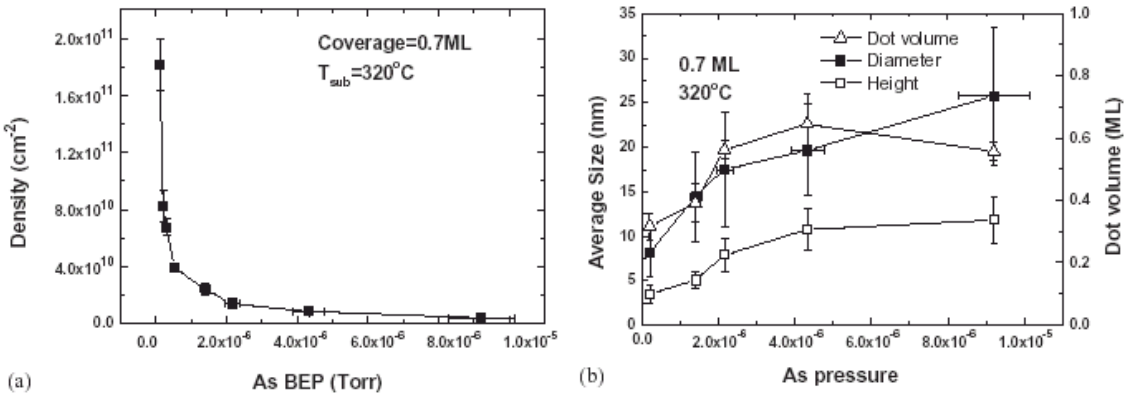

Figure 13. (a) Plot of InAs dot density dependence on arsenic BEP, (b) Plot of InAs dot size and volume dependence on arsenic BEP.

The well-reconstructed 2x1 surface completely disappears after InAs growth at low As BEP, indicating a highly "defective" As monolayer, i.e. with high density of As vacancies, as shown in Figure 14. The fact that high InAs dot density is obtained only at low As BEP supports the proposed mechanism.

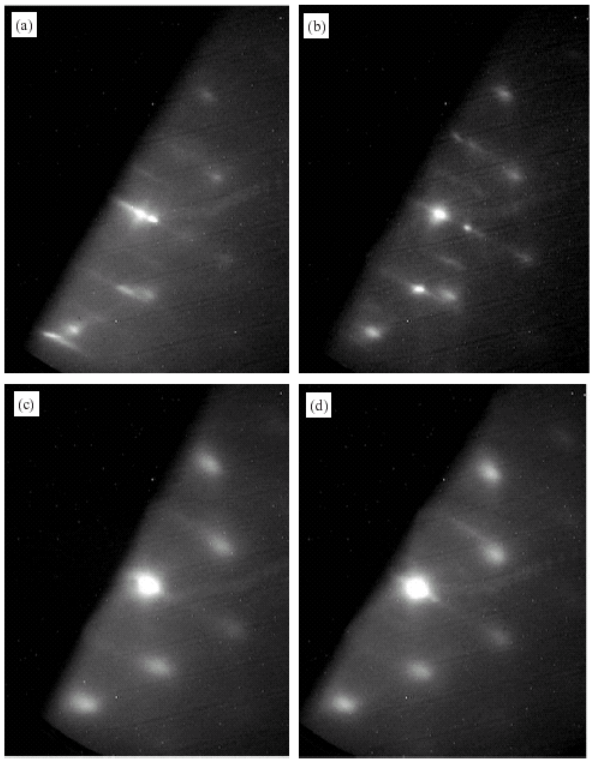

Figure 14. RHEED pattern of InAs growth with different arsenic BEP: a) 9.2×10^{-6} torr, b)1.4×10^{-6} Torr, c) 3.0×10^{-7} Torr, d) 1.2×10^{-7} Torr.

For temperature dependence study of dot formation,

The left side of figure 15 shows bright-field plan-view [001] TEM micrographs of samples grown at different substrate temperatures increased from 295 ^{o}C for a) to 410 ^{o}C for e). The right side of figure 15 is the histogram of size distribution based on the plan-view TEM. Gaussian curves were fitted on the size distribution histogram of figure 15. It is clear that increasing substrate temperature results in broadening of dot size distribution. Gaussian peak width, referd to as 0.849 full-width at half maximum (FWHM), increases from 8 nm to 14 nm when substrate temperature increases from 295 ^{o}C to 410 ^{o}C. Coarsening is likely to be responsible for the broadening of dot size distribution.

Figure 16 shows the dependence of dot density on substrate temperature. Dot density is nearly independent of substrate temperatures. The dot density at the onset of nucleation can be written for the well-studied quantum dot systems such as Ge/Si and InAs/GaAs [1,2] as follows[3]:

$$n \propto \left(\frac{F}{D_s}\right)^{\alpha} \qquad (1)$$

where F is the growth flux coming from source, D_s is the surface diffusion coefficient which increases exponentially ($D_s=D_0 exp(-E_a/k_BT)$) with increasing temperature. α is a constant associated mainly to the critical cluster size. α increases with increasing cluster size and saturates at unity for critical cluster size larger than 10 atoms. [4] For epitaxial growth, α can be treated as a constant.[14,15] n in equation (1) is the initial dot density. This simple model cannot explain the experimental observation that the dot density is nearly independent of temperature within the range of 295 ^{o}C to 410 ^{o}C under a constant arsenic BEP. This suggests that the nucleation model as in equation (1) that has been shown to be valid for Ge/Si and InAs/GaAs systems, does not apply to InAs growth on Si under our growth conditions.

[1] H. J. Kim, Z. M. Zhao, J. Liu, V. Ozolins, J. Y. Chang, Y. H. Xie, J. Appl. Phys. 95 (2004) 6065.
[2] K. Shiramine, T. Itoh, S. Muto, T. Kozaki, S. Sato, J. Cryst. Growth 242 (2002) 332.
[3] M. Schroeder, D. E. Wolf, Phys. Rev. Lett. 74 (1995) 2062.
[4] W. Theis, R. M. Tromp, Phys. Rev. Lett. 76 (1996) 2770.

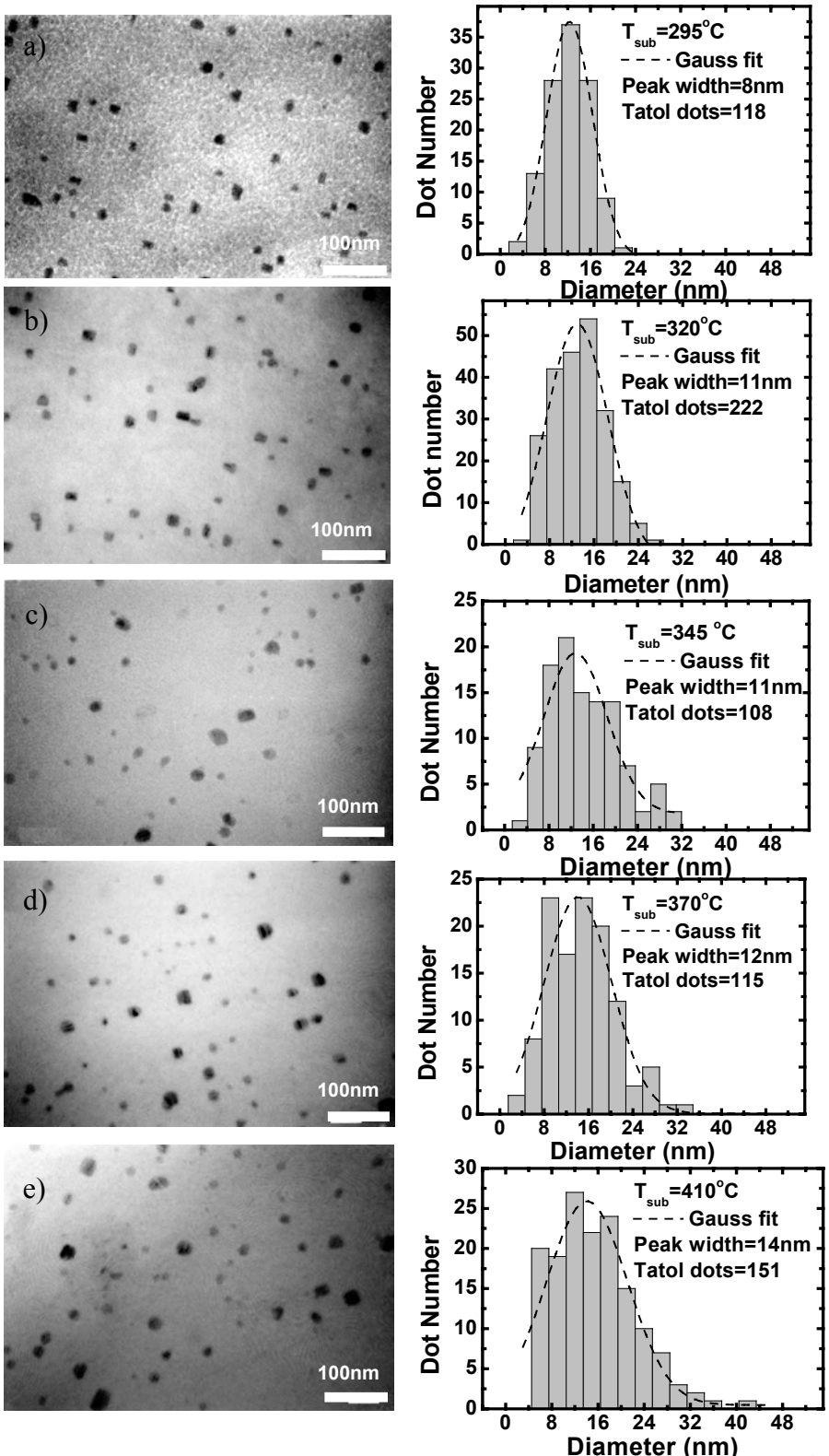

Figure 15. Plane-view [001] TEM images of InAs/Si quantum dots grown at a) 295°C, b) 320 °C, c) 345 °C, d)370 °C, e)410 °C.

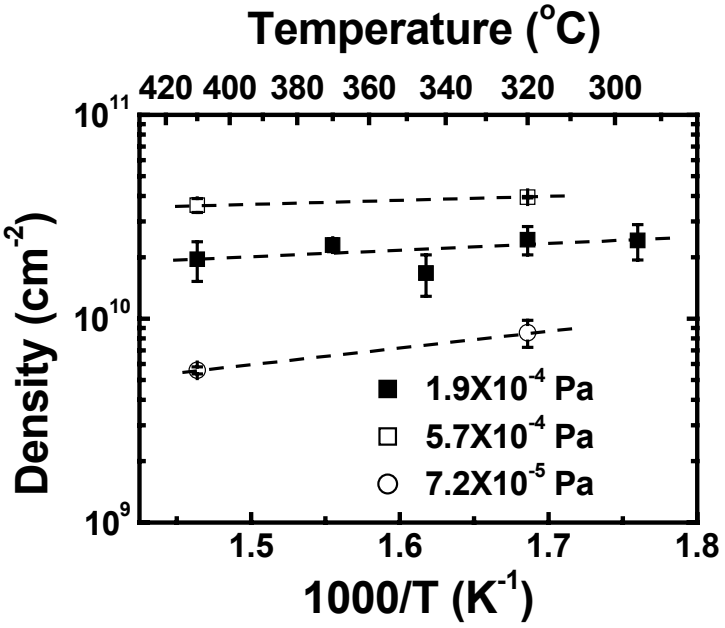

Figure 16. Arrhenius plot of InAs/Si dot density (y axis) dependence on substrate temperature (x axis).

Optimization of InAs quantum dots on Si.

High quality, narrow size distribution and high density dots can be achieved by InAs growth at lower temperature and lower arsenic BEP. In order to improve crystal quality and avoid the indium segregation under high temperature treatment, the dots growth is followed by annealing at higher temperature and higher arsenic BEP. The increase of RHEED intensity after growth and annealing, compared to samples grown at low temperature (below 250°C), confirmed the improvement of crystalline quality. Figure 17 (a) shows the plan-view TEM image of a sample that was grown at substrate temperature of 250°C with arsenic and indium BEP of 7.2×10^{-5} Pa and 7.6×10^{-6} Pa and annealed at substrate temperature of 410 °C with arsenic BEP of 1.9×10^{-4} Pa. The ramping time from 250 °C to 410 °C was set to 5 minutes. After the 120 second annealing at 410°C, the sample was cooled down to room temperature in approximately 10 minutes. This growth procedure resulted in QD density of 5.7×10^{10} cm^{-2}. The size distribution is shown in figure 17 (b). The Gaussian curve fitting of size distribution gives a narrow peak at around 11 nm with Gaussian peak width of 7 nm. The improvement in size distribution and the high density are attributed to low temperature growth and low arsenic BEP, respectively.

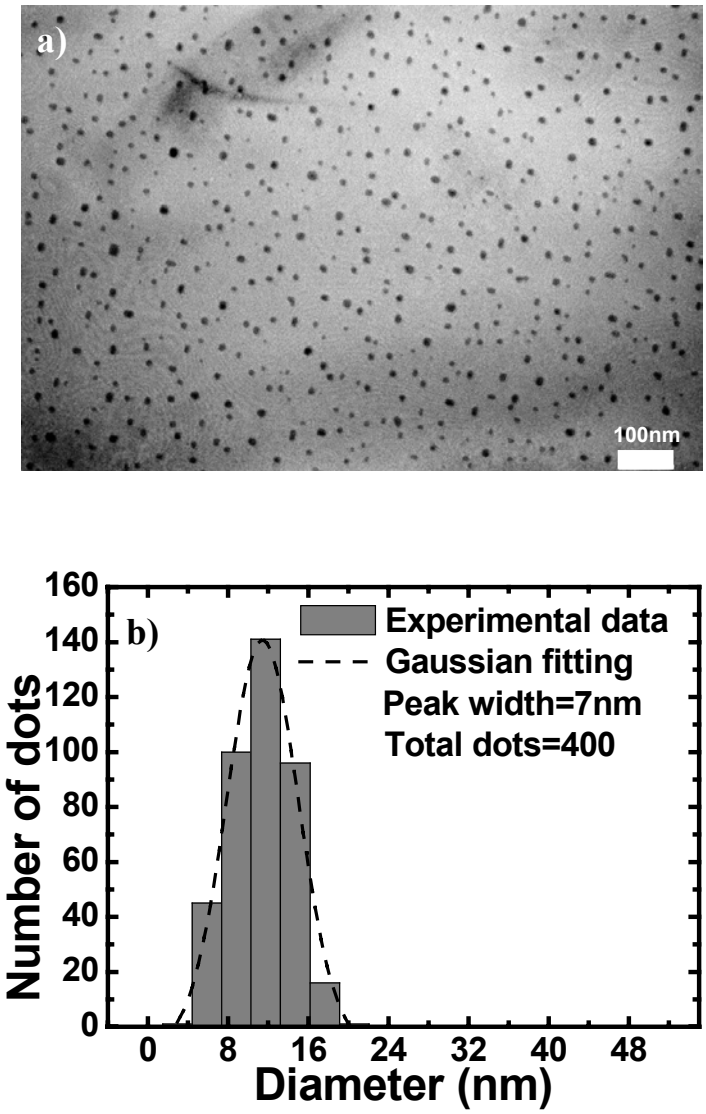

Figure 17. InAs dots grown on Si (100) at the substrate temperature of 250^{o}C and with arsenic BEP of 7.2×10^{-5} torr and post-annealed at 410^{o}C and 1.9×10^{-4} torr arsenic BEP: a) bright field plan-view [001] TEM micrograph and b) Histogram of size distribution of InAs dots.

InAs dot density dependence on III-V ratio:

InAs quantum dots were grown under different III/V ratio. The dot density change with III/V ratio is shown in the figure 18.

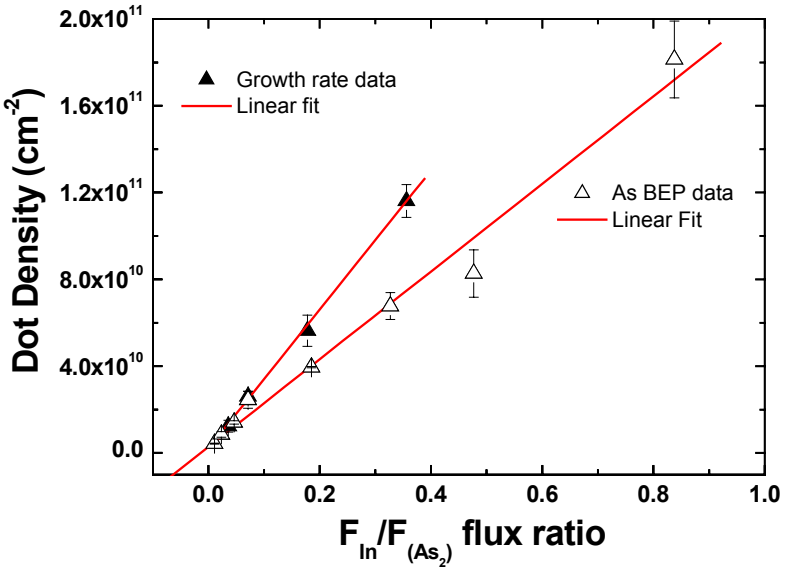

Figure 9. dot density dependence on III/V flux ratio. For the growth rate data the As BEP was kept at 1.4×10^{-6} Torr, for As BEP data growth rate was set at 0.02 ML/s. All growth was done at 320°C

The data from both constant As BEP and In BEP show the same trend that dot density is nearly linearly dependent on III/V flux ratio. This behavior provides a way to control the InAs dot density in a very large range from 10^9 cm^{-2} to 10^{11} cm^{-2}.

2). <u>Growth Mode of III-V on IV substrate</u>

From the growth of GaAs, InAs on Si and GaAs on Ge, we conclude that they are all in Volmer-Weber growth mode. Fig. 19 showed the reflection high-energy electron diffraction (RHEED) for the early stages (below 1 ML) of GaAs on Si (a), InAs on Si (b), GaAs on Ge (c). Fig. 19 (d) and (e) showed the RHEED pattern of Si and Ge surface before growth. It is very clear that the 3-dimensional island growth at very early stage (below 1 ML). Therefore all of the growth are Volmer-Weber growth without 2-dimensional wetting layer growth. Fig. 20 showed the AFM pictures of GaAs 0.7ML on Si (a), InAs 0.7 ML on Si (b). AFM data confirmed 3-D Volmer-Weber growth.

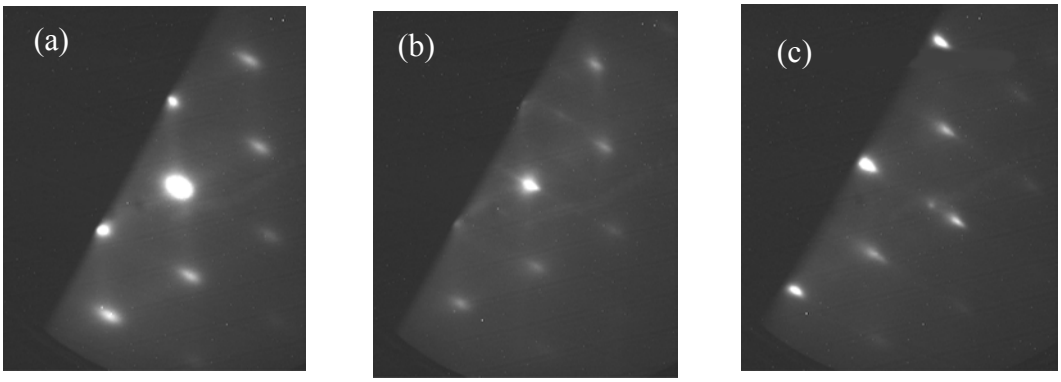

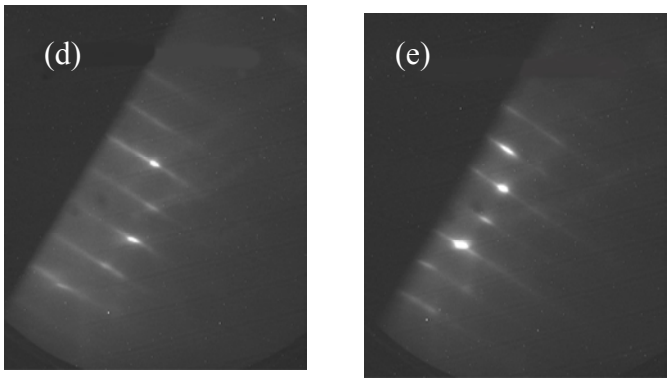

Fig. 19. RHEED images for different growth, (a)GaAs/Si at 320°C, (b) InAs/Si at 320°C, (c) InAs/Ge at 320°C, (d) Si surface before growth, (e) Ge surface before growth.

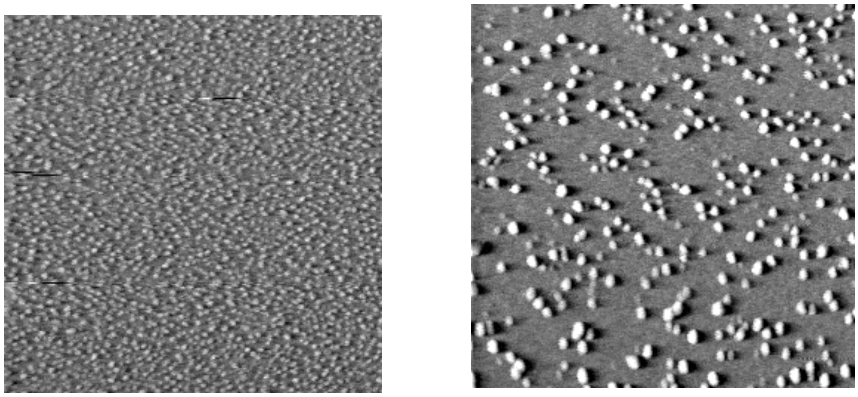

Fig. 20. 1 ×1 μm^2 AFM of GaAs (a) and InAs (b) growth on Si at the initial stages at InAs/Si at 320°C with arsenic BEP 1.4× 10^{-6} Torr.

3). First-principles calculations of different InAs overlayers on Si(001)

To understand the mechanism of initial stage of InAs grown on silicon (001) surface, first-principle total energy calculations were carried out with the plane-wave pseudopotential method within the generalized gradient approximation (GGA). A conjugate-gradient algorithm is used to minimizing the total energy therefore obtain the atom positions. Fig. 21 shows the positions of atoms in different systems with different InAs overlayers on silicon (001). We calculated the total energies of systems with different thickness of InAs on silicon substrate, which is shown in Table I. Comparing the total energy of two systems with the same number of atoms, while one system has half surface area covered with single As layer and half covered with As-In-As-In-As layer and another one with the whole surface covered with As-In-As layer, we can find the former one has a total energy of -(63.40+92.36)/2 eV = -77.88 eV, which is lower than the total energy (-77.82 eV) of system with a uniform As-In-

As layer. For a system with 1/3 area covered with As-In-As-In-As-In-As and 2/3 with single As, the total energy is –(106.97/3+63.40×2/3) eV = -77.92 eV, which is even lower. So the system prefers to form InAs islands with As-finished silicon surface rather than uniform InAs layer on silicon surface, which causes a 3D growth mode of InAs on silicon even in the very initial stage. In the real case, since the island formation in 3D growth will partially release the strain energy that is comes from the lattice mismatch between InAs and Si, the 3D growth will be even more energy favorable.

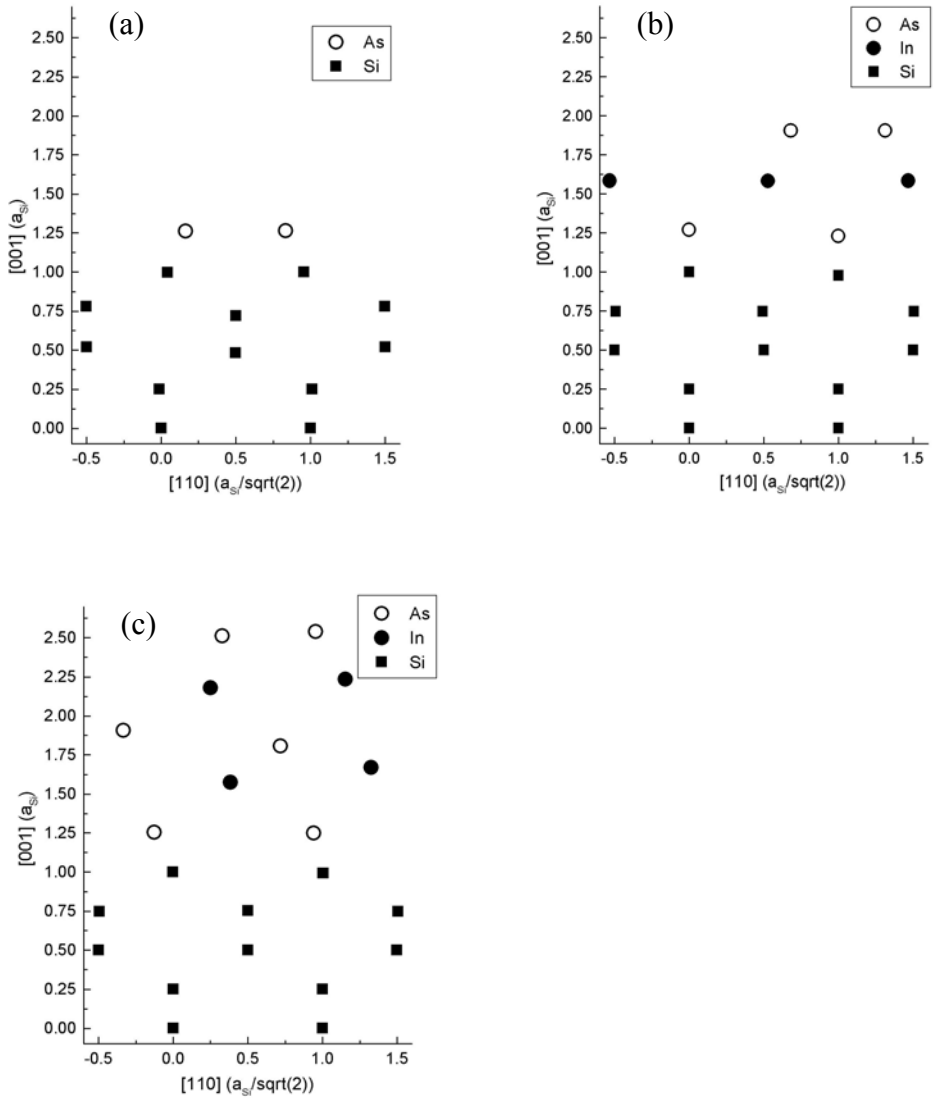

Fig. 21. Calculation positions of atoms in (a) Si(001)-As, (b) Si(001)-As-In-As and (c) Si(001)-As-In-As-In-As.

TABLE I. Total energies of systems with different InAs overlayers on silicon. The unit area used in the table is the area for one surface dimmer.

Structure	Total energy (eV/unit area)
Si(001)-As	-63.40
Si(001)-As-In-As	-77.82
Si(001)-As-In-As-In-As	-92.36
Si(001)-As-In-As-In-As-In-As	-106.97

4) <u>Critical size of threading dislocation-free dots at different growth conditions:</u>

1. Critical size dependence on arsenic BEP

Plastic relaxation in strained InAs islands grown on Si (001) by MBE as a function of arsenic beam equivalent pressure is investigated using transmission electron microscopy. Analyses of the spacing in Moiré fringes show a clear trend of larger InAs lattice parameters with increasing island size as a result of the elastic relaxation of three-dimensional structures. Our experimental findings show: (1) the existence of a critical lattice parameter (0.597 ±0.01nm) instead of a critical island size that determines the onset of dislocation, and (2) a clear dependence of the critical size of InAs clusters on arsenic BEP during MBE growths from 1.2×10^{-7} to 9.2×10^{-6} Torr. We postulate that these results are the consequences of the As BEP dependent surface energy of the various facets and the associated InAs island shape change.

Fig. 22 showed the dark-field plan-view TEM images of InAs dots grown under different arsenic BEP. The Moiré fringes of each dot can be accurately determined from images. The lattice parameters can be obtained from spacing of Moiré fringes.[5,6] The dislocation can be identified from the terminated Moiré fringe.[7]

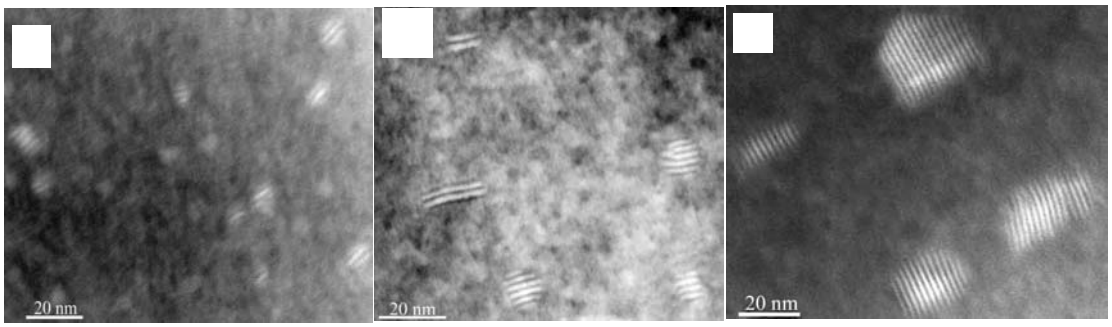

Fig. 22 Dark field (**g** = 220) plan-view TEM micrographs of InAs islands on Si (001) substrate with As pressure equal to 1.2×10^{-7} Torr (A), 1.4×10^{-6} Torr (B) and 9.2×10^{-6} Torr (C). Samples are grown at 320ºC with 0.7ML InAs coverage

[5] P.D. Miller, C.P. Liu, W.L. Henstrom, J.M. Gibson, D.G. Cahill, Y. Huang, P. Zhang, T.I. Kamins, D.P. Basile, R.S. Williams, Appl. Phys. Lett. 75 (1999) 46.
[6] P. Chen, Q. Xie, A. Madhukar, Li Chen, A. Konkar, J. Vac. Sci. Technol. B 12 (1994) 2568.
[7] "Electron Microscopy of Thin Crystals," P. Hirsch, A. Howie, R.B. Nicholson, D.W.Pashley, and M.J. Whelan, (Robert E. Krieger, New York, 1977), p.372.

The size distribution of both dislocation-free dots and dislocated dots was shown in Fig. 22. It is very clear that the relative percentage of relaxed versus strained islands increases monotonically with BEP_{As} (from 15% of dislocated InAs islands for the lowest As BEP to 70% for the highest As BEP)

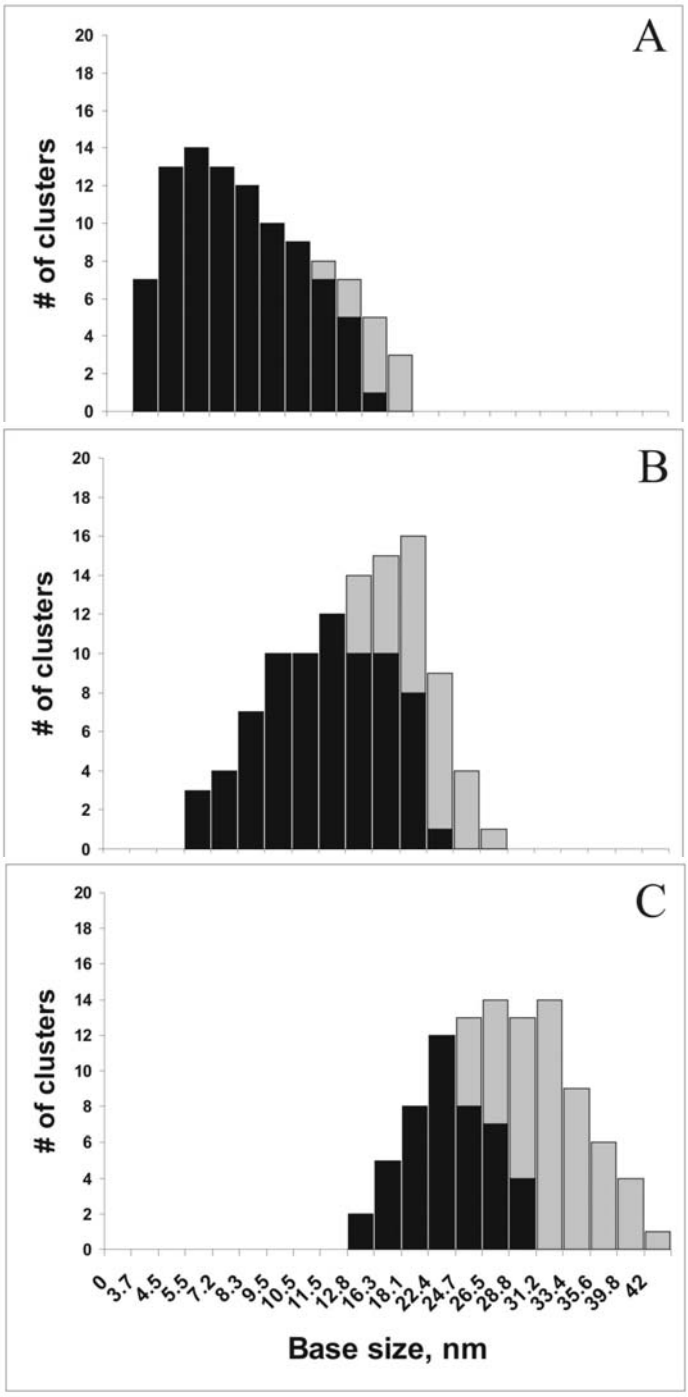

Fig 23. The histograms of dislocation-free (black) and dislocated (gray) islands as function of their base sizes corresponding to the same set of samples as in Fig.22.

The critical sizes of dislocation-free dots grown under different arsenic BEP are shown in Fig. 24. The critical base size dimensions of coherent islands increases significantly (from 13 to 28 nm) with increasing arsenic BEP from 1.2×10^{-7} Torr to 9.2×10^{-6} Torr.

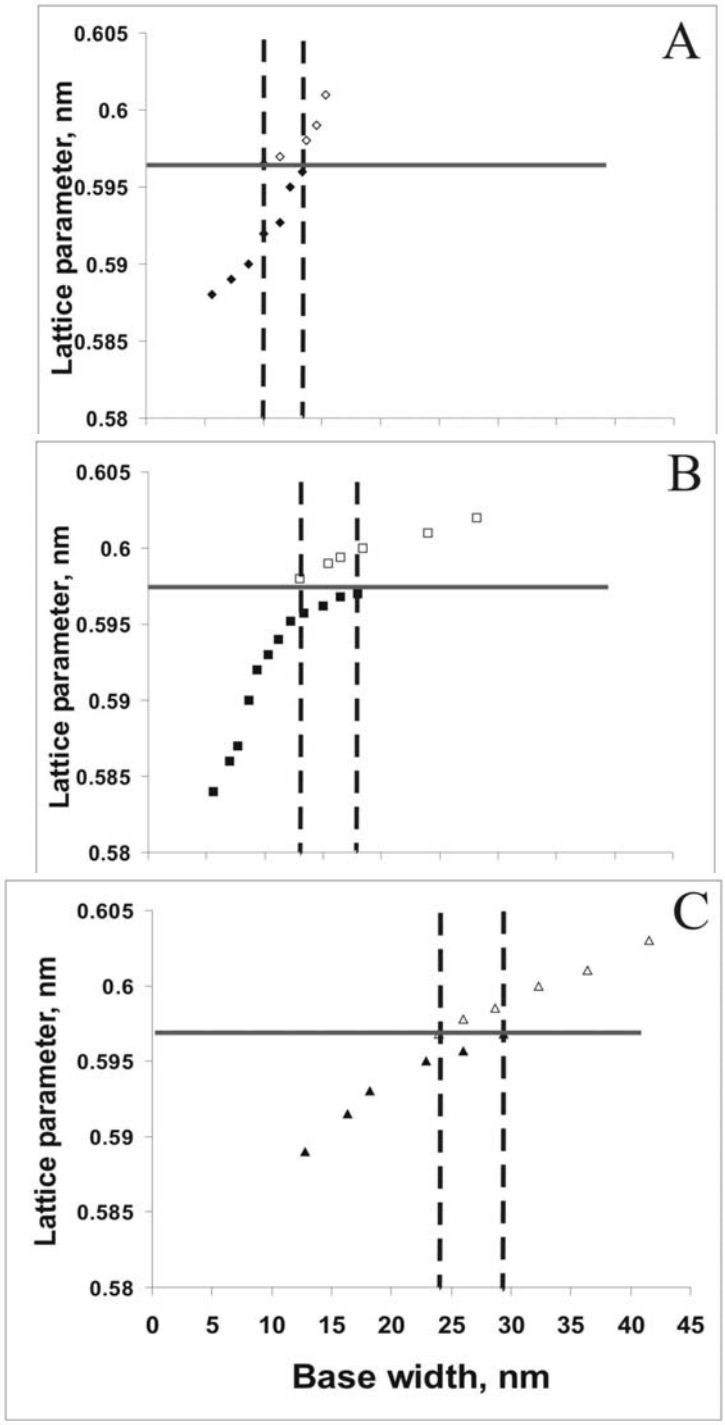

Fig. 24 The average in-plane lattice parameter of InAs islands as a function of their base sizes for the same set of samples as in Fig.22. Dislocation occurs at a well defined a = 0.597±0.01 nm (as indicated by horizontal lines) and is relatively independent of island sizes.

2. Critical size dependence on substrate temperature

Relaxation of InAs islands epitaxially grown by molecular beam epitaxy on Si (001) as a function of the substrate temperature is investigated using transmission electron microscopy. Analysis of the spacing in Moiré fringes shows that an increase in the average InAs lattice parameters with increasing island sizes in both elastically as well as plastically relaxed islands. Using this method, a critical InAs islands size for dislocation is determined to be 13.5±0.1 nm, with a corresponding critical InAs lattice spacing of 0.579±0.01nm along ⟨011⟩ crystallographic directions. The critical dimensions are independent of the substrate temperature. Although no dislocations can be observed in islands smaller than the critical size, the size of the largest dislocation-free islands does increase significantly (from ~17 nm to ~24 nm) with increasing substrate temperature (from 295ºC to 410ºC).

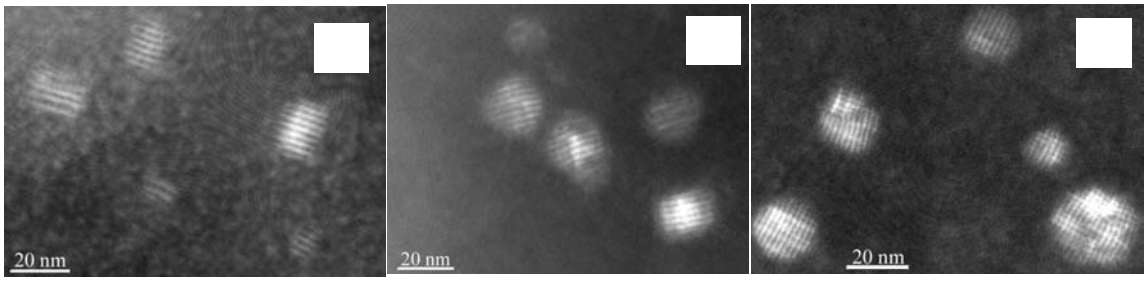

Fig.25 Dark field (**g** = 220) plan-view TEM micrographs of InAs islands on Si (001) substrate for samples grown with As pressure equal to 1.4×10^{-6} Torr with total coverage 0.7ML at substrate temperatures 295ºC (A), 345ºC (B) and 410ºC (C), respectively.

Fig.25 shows typical plan-view TEM micrographs of samples grown at three different temperatures: 295ºC, 345ºC and 410ºC, respectively. It is apparent that increase in substrate temperature within this range leads to a slight decrease in the average density of InAs islands, owing presumably to the increased surface diffusion of InAs and the associated coarsening. There is indeed a clearly broadening of InAs island size distribution as can be visible by comparing Fig. 26 A, B and C. Calculated values of $\boldsymbol{a_{isl}}$ are plotted as a function of the island base sizes in Fig. 27 A, B and C. Both strained (closed symbols) and relaxed (open symbols) islands are considered. The ratio of relaxed to strained islands increases from 20 to 35% with an increase of substrate temperature from 295ºC to 410ºC. There is a corresponding increase in the average dots size as can be seen from Fig.26 A, B and C. An important feature of Fig.26 is that the size distribution of coherent islands is nearly temperature independent. The substrate temperature increase results primarily in a broadening of the range of island sizes within which coherent and dislocated islands coexist. This range is from 13.7 nm -17.5 nm from samples grown at 295ºC. It increases to from 13.7 nm – 24 nm for samples grown at 410ºC.

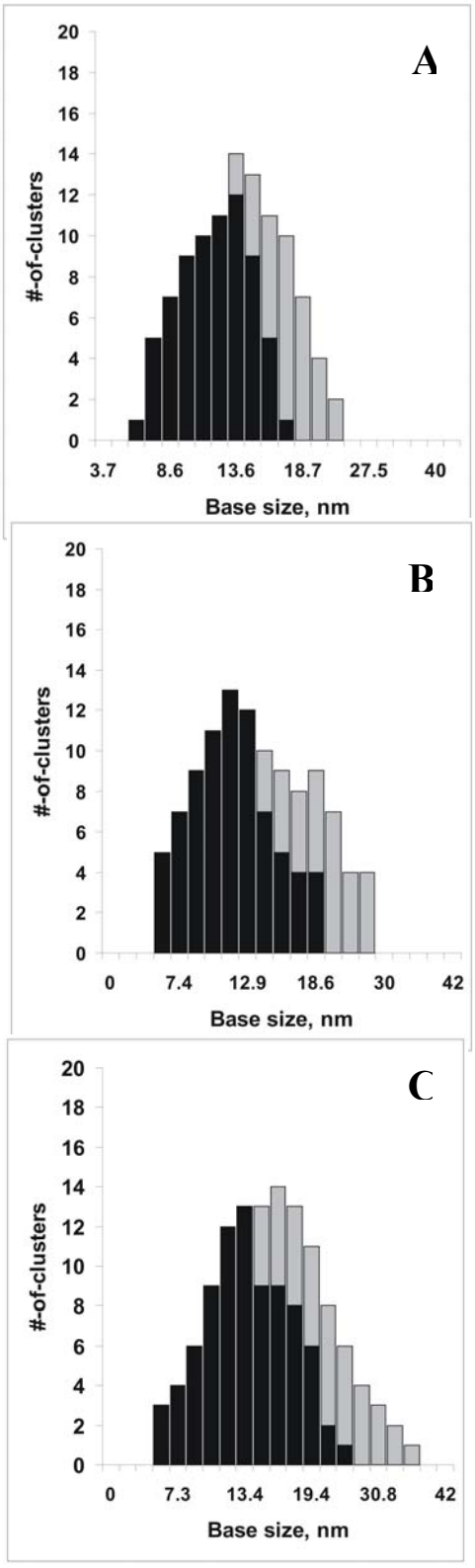
A
#-of-clusters
20
18
16
14
12
10
8
6
4
2
0
3.7
8.6
13.6
18.7
27.5
40
Base size, nm
B
#-of-clusters
0
7.4
12.9
18.6
30
42
Base size, nm
C
#-of-clusters
0
7.3
13.4
19.4
30.8
42
Base size, nm

Fig. 26 InAs islands size distribution that corresponds to the same set samples as in Fig.25, showing number of coherent (black) and incoherent (gray) islands as function of their base size.

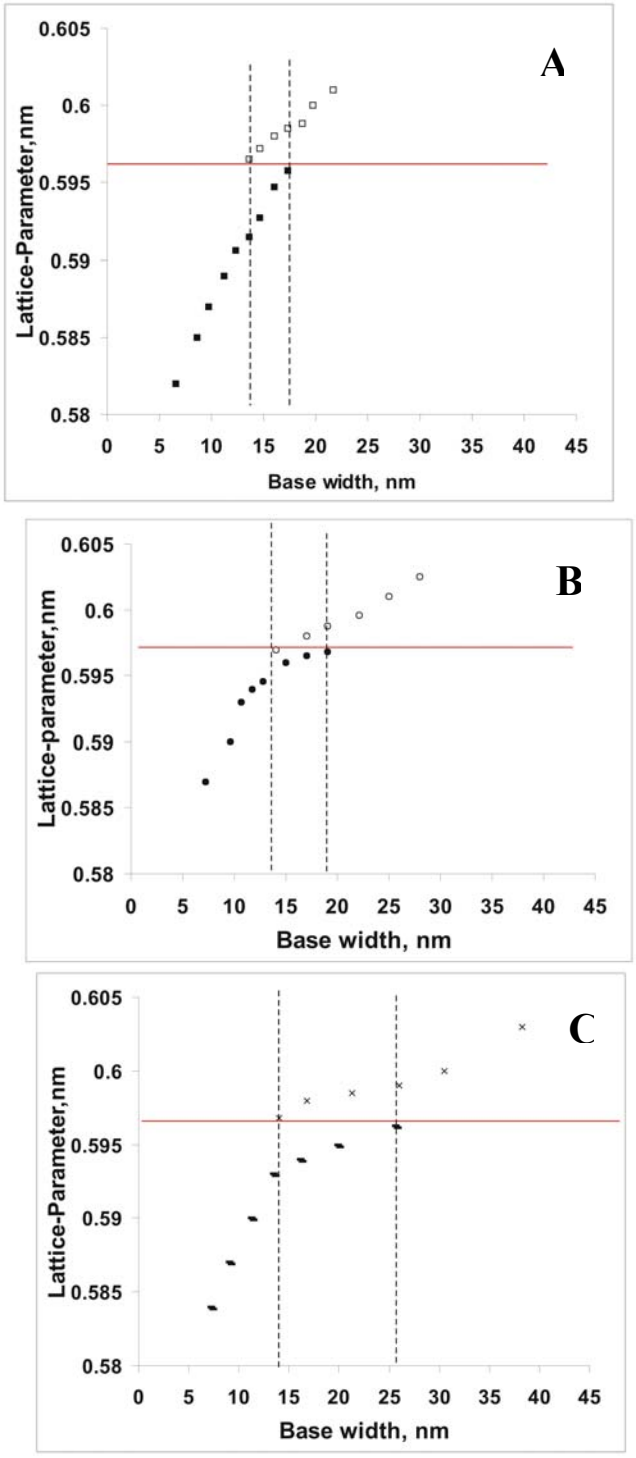

Fig. 27 Plots of an average in plane lattice parameter of InAs islands as a function of their base size for the same set samples as in Fig.25. Horizontal line corresponds to the critical island lattice parameter that

indicates the upper limit for the coherent islands. Vertical dashed lines show regions where both coherent and incoherent islands exist.

5) <u>InAs growth on relaxed SiGe buffer layer</u>

InAs dots were grown on relaxed SiGe buffer layer. Fig. 28 shows the typical sample structure. Fig. 29 showed AFM images of Ge dots on relaxed SiGe buffer layer and InAs dots on relaxed SiGe buffer layer. It is very interesting to notice that InAs dots do not preferentially nucleated over the dislocation network. Comparing to Ge dots on relaxed buffer layers, the growth mode is VW instead of SK and the misfit strain is increased from 4% to 11% for InAs on Si. Which one of these two factors prevents the InAs dots from registering to the underlying dislocation network is an important question to answer. We plan on conducting studies using GaAs on SiGe to single out the chemical incompatibility from the misfit strain in an effort to hunt for the answer to this question.

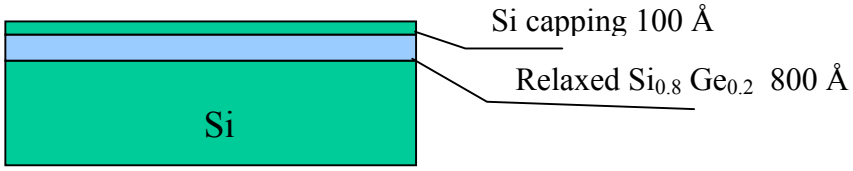

Fig.28, The substrate structure with dislocation network.

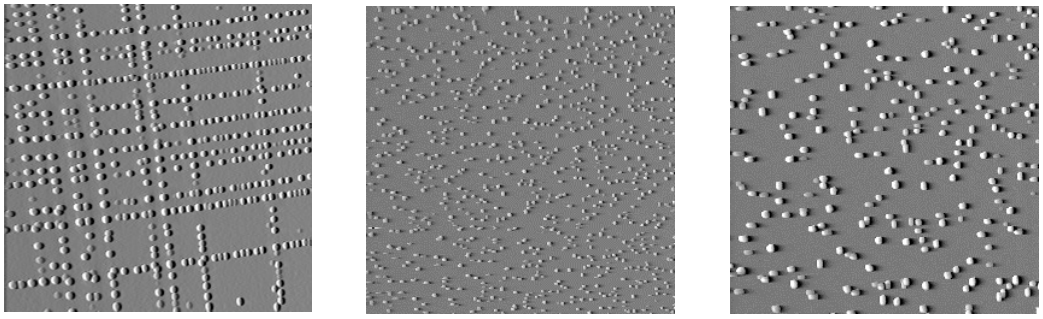

(a) Ge/ Si (b) InAs/ Si (c) InAs/Si

Fig. 29. (a) $5\times5\mu m^2$ AFM image of Ge quantum dots on Si, (b) $5\times5\mu m^2$ AFM image of InAs quantum dots on Si, (c) $3\times3\mu m^2$ AFM image of InAs quantum dots on Si.

6) <u>Contrast between InAs and GaAs on Si (001)</u>

Both InAs and GaAs are grown on Si (001) with the similar growth conditions. A clear difference between the InAs and GaAs growth behavior is the dot density dependence on arsenic BEP. InAs dot density strongly depends on the arsenic BEP, while GaAs dot density is nearly independent on arsenic BEP, as figure 30 shown. This suggests that there is fundamental physical difference between the InAs and GaAs grown on Si (001).

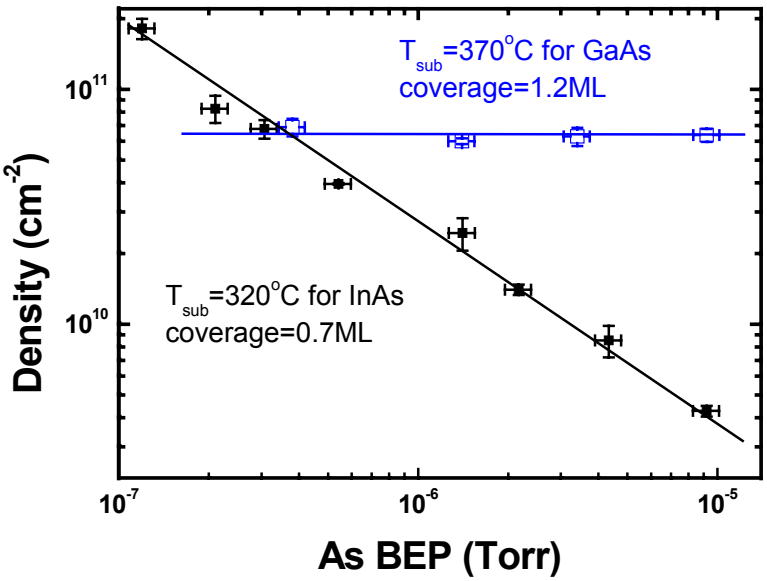

Figure 30. The blue line is the GaAs dot density and black line is the InAs dot density. The growth rate is 0.01 ML/s for GaAs and 0.02 ML/s for InAs. Because the 0.02 ML/s growth rate for GaAs growth is too high to distinguish the dots.

7) <u>High resolution transmission electron microscopy study of InAs on Si (001)</u> :
The detailed structure of InAs on Si(001) is studied via high resolution TEM. The strain is relieved by introducing misfit dislocation at very early growth stages, with island size larger than 4nm, as shown in Fig. 31. Both glissile 60 ^{o} dislocation and sessile 90 ^{o} dislocations are observed by TEM. At the beginning of dislocation formation, the 60 ^{o} dislocation is formed. With increasing size of island, the 90^{o} dislocations appear. It is very likely that the 90^{o} dislocations are formed by two 60^{o} dislocation with increasing dislocation number, as shown in Fig. 32

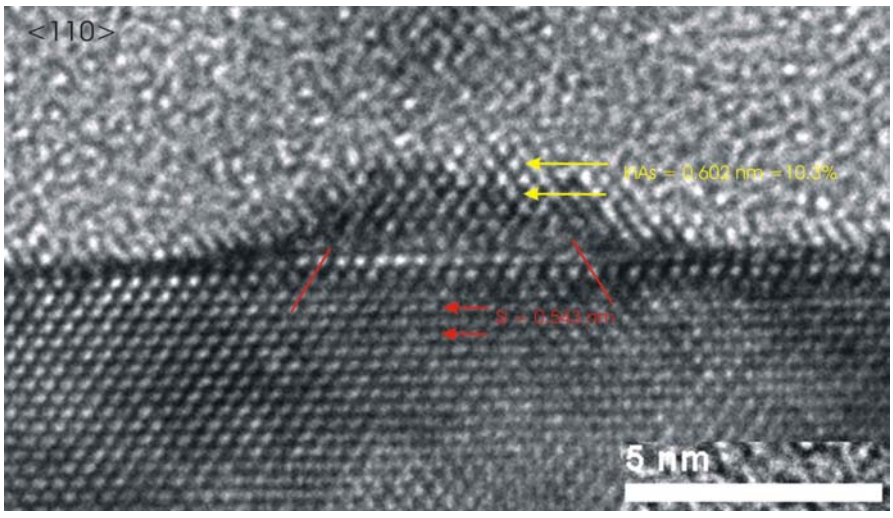

Figure 31. 60^{o} misfit dislocations formed at the interface (indicated by red lines).

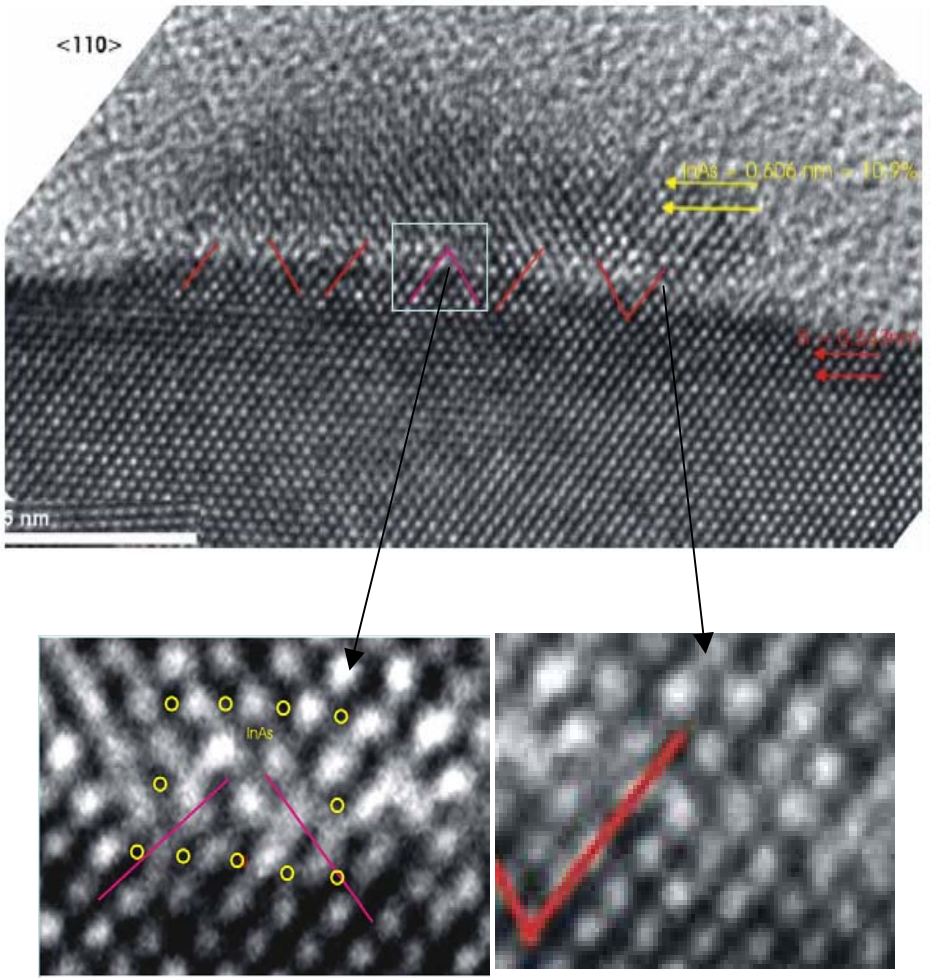

Figure 32. Both 60^{o} and 90^{o} dislocations formed at the interface between Si and InAs. The enlarged images show the detailed atomic structure of dislocations.

Summary

We have demonstrated the key parts of a Si-based laser structure with optimized design. Relatively low propagation loss was achieved even in a SiGe waveguide with metal cladding, high injection current of more than 2 kA/cm^2 can be easily achieved in such a low loss waveguide, and single mode resonance was achieved in a SiGe DBR resonant cavity. In addition, we have carried out theoretical calculation for coupled SAQD systems and formulated the distinct advantage of a coupled SAQD system for laser applications. We also achieve controllable growth of InAs quantum dots on silicon, and a detail study of structure characteristics of such quantum dots was carried out.

The crucial finding from this program is that the very small critical size of InAs SAQD for dislocation and the associated extreme quantum confinement show that there might not be a window in the dot size for which electron-hole pairs can be confined and the dots are coherently strained. It can be used as a guide for future funding decisions on the subject of lasers on Si.

Publications

"Effects of growth temperature and arsenic pressure on size distribution and density of InAs quantum dots on Si (001)" Z. M. Zhao, O. Hul'ko, H. J. Kim, J. Liu, B. Shi and Y. H. Xie, Thin Solid Film, (to be published)

"Growth and characterization of InAs quantum dots onSi(0 0 1) substrates" Z.M. Zhao, O. Hul'ko, H.J. Kim, J. Liu, T. Sugahari, B. Shi, Y.H. Xie, J. Cryst. Growth, 271, 450 (2004)

"A technique for the measurement of surface diffusion coefficient and activation energy of Ge adatom on Si(001)" H. J. Kim, Z. M. Zhao, J. Liu, V. Ozolins, J. Y. Chang, and Y. H. Xie, J. Appl. Phys. 95, 6065 (2004)

"On the formation mechanism of epitaxial Ge islands on partially relaxed SiGe buffer layers" H. J. Kim, J. Liu, Z. M. Zhao, and Y. H. Xie, J. Vac. Sci. Technol. B 22, 2257 (2004)

"Influence of coupling effect in the operation of vertically coupled quantum-dot lasers", B. Shi and Y. H. Xie, Appl. Phys. Lett., 82, 4788 (2003).
Also be selected for the July 7, 2003 issue of the Virtual Journal of Nanoscale Science & Technology

"Three-stage Nucleation and Growth of Ge Self-Assembled Quantum Dots Grown on Partially Relaxed SiGe Buffer Layers", H.J. Kim, Z.M. Zhao, and Y.H. Xie, Phys. Rev. B 68, 205312 (2003)

"Influence of a buried misfit dislocation network on the pyramid-to-dome transition size of Ge self-assembled quantum dots on Si(001)," H.J. Kim, J.Y. Chang, and Y.H. Xie, J. Cryst. Growth, Vol. 247, 251 (2003);

"Influence of the wetting-layer growth kinetics on the size and shape of Ge self-assembled quantum dots on Si(001)," H.J. Kim and Y.H. Xie, Appl. Phys. Lett. **79**, 263 (2001).

Talks

"Three-stage nucleation and growth of Ge self-assembled quantum dots grown on partially relaxed SiGe buffer layers" HyungJun Kim, ZuoMing Zhao, Ya-Hong Xie, Material Research Society Spring Meeting, San Francisco, April 14, 2004

"InAs quantum dots growth on Si (001) substrates" The Workshop on Compound Semiconductor Materials and Devices, Pasadena, Zuoming Zhao Ya-hong Xie, California February 15-18, 2004.

"Understanding the Physics of Self-assembled by Epitaxy of Quantum Dots of Cubic Semiconductors" The 4th International Workshop on Semiconductor Quantum Structures and Nano-Photonics, HyungJun Kim, ZuoMing Zhao, Joon-Yeon Chang, Ya-Hong Xie, Korea, November 26, 2003

" A novel technique for the measurement of ge adatom surface migration length on Si (001)" H. J. Kim, Joon-Yeon Chang, Y. H. Xie, Material Research Society Spring Meeting, San Francisco, April, 2002.

"Fabrication of self-assembled quantum dots in cubic semiconductor materials for device applications", Ya-Hong Xie, presented at the Workshop of the Institute for Pure and Applied Mathematics (IPAM), Lake Arrowhead, CA, December 2002 (invited);

"The influence of a buried misfit dislocation network on the pyramid-to-dome transition size in Ge self-assembled quantum dots on Si(001)", H.J. Kim, J.Y. Chang, and Y.H. Xie, June 22, 2001, Electronic Materials Conference, South Bend, IN;

"Fabrication of Self-assembled Quantum Dots", Y.H. Xie, March 28, 2001, Naval Research Laboratory, Electronics Science and Technology Seminar, Washington DC (INVITED);

People supported by this program (100% and/or partially)

Ya-Hong Xie	PI (partial)
Oksana Hul'ko	Postdoc (partial)
HyungJun Kim	Graduate student (partial)
Bin Shi	Graduate student (partial)
Jian Liu	Graduate student (partial)
ZuoMing Zhao	Graduate student (partial)